# Electronic Supporting Information (ESI)

# Significant Adsorption Enhancements Driven by Pore Microenvironment Tuning for Efficient $C_2H_2/C_2H_4$ Separation in a Chemically Stable $Ni_7$-Cluster-based framework

Yunli Wang, [a] Rizhao Zhang,[a] Jin-peng Xue,[a] Yuqiao Chai,*[b] Bao Li,*[c] and Jia Li*[a]

[a] *School of Materials Science and Chemical Engineering, Ningbo University, Ningbo, Zhejiang 315211, China. E-mail: lijia@nbu.edu.cn*

[b] *School of Material and Chemical Engineering, Ningbo University of Technology, Ningbo, Zhejiang 315211, China. E-mail: chaiyuqiao@nbut.edu.cn*

[c] *Key Laboratory of Material Chemistry for Energy Conversion and Storage, School of Chemistry and Chemical Engineering, Huazhong University of Science and Technology, Wuhan, Hubei 430074, China. E-mail: libao@hust.edu.cn*

## Materials and methods.

### Chemicals.

All chemicals were purchased from commercial sources and were used without further purification ：Isonicotinic acid (aladdin), isophthalic acid (aladdin), $Ni(NO_3)_2 \cdot 6H_2O$ (aladdin) NaOH (Sigma-Aldrich).

**Synthesis of Ni7-MOF.** Ni7 was synthesized by a hydrothermal method. Isonicotinic acid (0.025 g, 0.2 mmol), isophthalic acid (0.0664 g, 0.4 mmol), NaOH (0.045 g, 1.1 mmol) were mixed in an aqueous solution (10 mL), then solid $Ni(NO_3)_2 \cdot 6H_2O$ (0.206 g, 0.7 mmol) was poured into a 25 mL Teflon vessel, and heated to 185 °C for 3600 min. After cooling to 30 °C, green block crystals were obtained by filtration.

**Scalable synthesis of Ni7-MOF:** Isophthalic acid (0.66 g), isonicotinic acid (0.25 g), NaOH (0.45 g) and deionized water (50 mL) were added to a 100 mL Teflon vessel, stirred until all organic ligands were dissolved, then Add $Ni(NO_3)_2 \cdot 6H_2O$ (1.5 g) and heated to 185 °C for 3600 min. After cooling to room temperature, green block crystals were obtained by filtration.

### Gas sorption experiment

Gas sorption isotherms were performed on Micromeritics (3FLEX) aparatus. Prior to the adsorption testing, the freshly synthesized Ni7-MOF underwent a water-washing process, followed by vacuum activation for four hours at temperatures of 100°C and 250°C. This treatment yielded two distinct desolvated structures, designated as Ni7-100 and Ni7-250. The permanent porosity of the two desolvated structures were checked by $N_2$ adsorption at 77 K and $CO_2$ adsorption at 195 K.

### Breakthrough tests

The breakthrough experiments were carried out in homemade dynamic gas breakthrough equipment. A stainless steel column (4.6 mm inner diameter × 50 mm) packed with fully activated samples (0.905g for Ni7-100, and 0.9775g for Ni7-250) was firstly purged with He flow (5 ml min$^{-1}$) for 0.5 h at 293K. The mixed $C_2H_2/C_2H_4$ (1/1, 1/9, and 1/19, v/v) gas flow was introduced under different testing temperatures and flow rates to validate the actual separation efficiency. The relative amounts of the gases passing through the column were monitored using gas chromatography (Agilent 7890B) with a thermal conductivity detector (TCD) once every 30 seconds, after 180 minutes, the test becomes to once every 5 minutes. After every separation experiment, the adsorption bed was regenerated by heating at 70 °C under vacuum conditions for 2 hours. We store the used sample in the sample tube, and the tube is kept in the refrigerator at about 5 °C for more than half a year. The recycling breakthrough experiments were performed using the used samples under the same conditions after the same activation.

### IAST adsorption selectivity calculation:

The experimental isotherm data for pure $C_2H_2$ and $C_2H_4$ (measured at 273 K) were fitted using a Langmuir-Freundlich (L-F) model:

$$q = \frac{a * b * p^c}{1 + b * P^c} \quad (2)$$

Where q and p are adsorbed amounts and pressures of component i, respectively. Using the pure component isotherm fits, the adsorption selectivity is defined by

$$S_{ads} = \frac{q_1/q_2}{p_1/p_2} \quad (3)$$

Where $q_i$ is the amount of i adsorbed and $p_i$ is the partial pressure of i in the mixture.

We used the following written codes to simulate the adsorption selectivity of $C_2H_2/C_2H_4$ in Fig. 2:

28          # No. of Pressure Point

y1, y2      # Molar fraction of binary mixture (y1 and y2, y1 + y2 = 1)

1, 2, 3, 4, 5, 6, 7, 8, 9, 10, 20, 30, 40, 50, 60, 70, 80, 90, 100, 101, 102, 103, 104, 105, 106, 107, 108, 109          #The unit is same parameter b, kPa

a1, a2     # fitting parameter Nsat (A1) for both component (Unit: mmol/g)

b1, b2      # fitting parameter b1 for both components (Unit: kPa$^{-1}$)

c1, c2     # fitting parameter c1 for both components

0, 0      # fitting parameter Nsat2(A2) for both component(Unit: mmol/g)

0, 0      # fitting parameter b2 for both components (Unit: kPa$^{-1}$)

1, 1      # fitting parameter c2 for both component

**Calculation of breakthrough selectivity**

The gas adsorption quantity (qi) is calculated from the breakthrough curve using the following formula:

$$breakthrough\ selectivity = \frac{q_A/y_A}{q_B/y_B} \quad (4)$$

where qi is the adsorption capacity of gas i (mmol/g) and yi is the molar fraction of gas i (i=A, B) in the gas mixture.

The gas adsorption capacity is determined as follows:

$$q_i = \frac{f_i(t_1 - t_0) - f_j \int_{t_0}^{t_1} F_i(t)dt}{22.4 \times M} \quad (5)$$

Where $f_i$ and $f_j$ are the flow rates of gas i and j (mL min$^{-1}$ ), respectively; $t_0$ and $t_1$ are the initial time and the final time of the experiment (min), respectively; $F_i(t)$ and $F_j(t)$ are the functions of the breakthrough curves of components i and j, respectively, and M is the mass of the adsorbent (g).

The pure alkene volume per volume or weight of materials was obtained by the following equation,

$$V_{Pure} = \frac{f_j \int_{t_0}^{t_1} F_j(t)dt}{M/\rho} \qquad \text{(based on volume of adsorbent)} \qquad (6)$$

$$V_{Pure} = \frac{f_j \int_{t_0}^{t_1} F_j(t)dt}{M} \qquad \text{(based on weight of adsorbent)} \qquad (7)$$

where $f_j$ is the flow rate of gas j (alkene) (mL/min), respectively; $t_0$ and $t_1$ are the initial time and the final time for only pure gas j being detected (min), respectively; $F_j(t)$ is the function of the breakthrough curve of component j; M is the mass of the adsorbent; $\rho$ is the density of the adsorbent.

**Calculations and simulation details**

All Gas adsorption simulations were performed using the Sorption model, within the Compass III force field. The electrostatic and van der Waals were Ewald and Atom based respectively. The adsorption process was simulated at 298 K and 1 bar. The generalized gradient approximation (GGA) method with Perdew-Burke-Ernzerhof (PBE) function was employed to describe the interactions between core and electrons. The force and energy convergence criterion were set to 0.002 Ha Å$^{-1}$ and 10$^{-5}$ Ha, respectively. The GCMC simulations which were carried out to investigate the adsorbed capacity of MOFs at 298 K and 1 bar were performed by Sorption mode, within the Compass III force field. A simulation box with a 1×1×1 crystallographic unit cell was used. The electrostatic and van der Waals were Ewald and Atom based respectively. The adsorption process was simulated at 298 K and 1 bar. A simulation box with a 1×1×1 crystallographic unit cell was used. During the simulations, in order to guarantee the equilibration and to sample the desired properties, 2×10$^7$ steps were performed. In all simulations, we employed a rigid framework assumption.
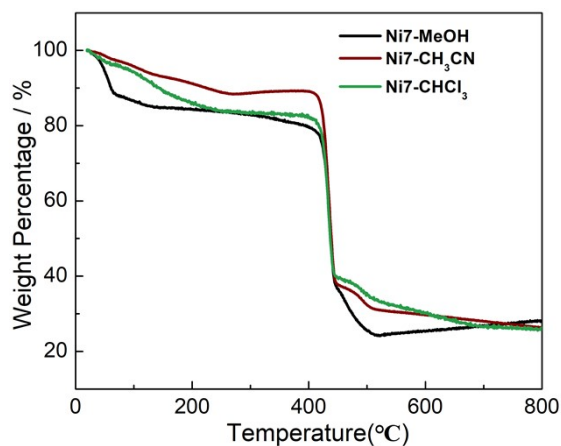
**Additional Figures**

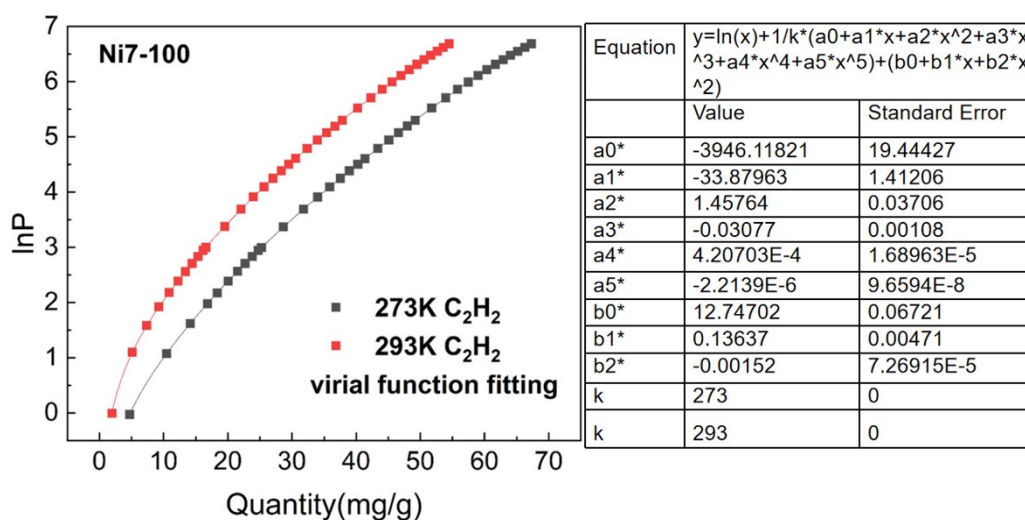**Fig. S1** TGA curves of Ni7-MOF after different solvent exchanges.



| Equation | y=ln(x)+1/k*(a0+a1*x+a2*x^2+a3*x^3+a4*x^4+a5*x^5)+(b0+b1*x+b2*x^2) | |
|----------|--------|----------------|
|  | Value | Standard Error |
| a0* | -3946.11821 | 19.44427 |
| a1* | -33.87963 | 1.41206 |
| a2* | 1.45764 | 0.03706 |
| a3* | -0.03077 | 0.00108 |
| a4* | 4.20703E-4 | 1.68963E-5 |
| a5* | -2.2139E-6 | 9.6594E-8 |
| b0* | 12.74702 | 0.06721 |
| b1* | 0.13637 | 0.00471 |
| b2* | -0.00152 | 7.26915E-5 |
| k | 273 | 0 |
| k | 293 | 0 |

**Fig. S2** The $C_2H_2$ fit isotherms of Ni7-100 at 273 K and 293 K by virial equation.



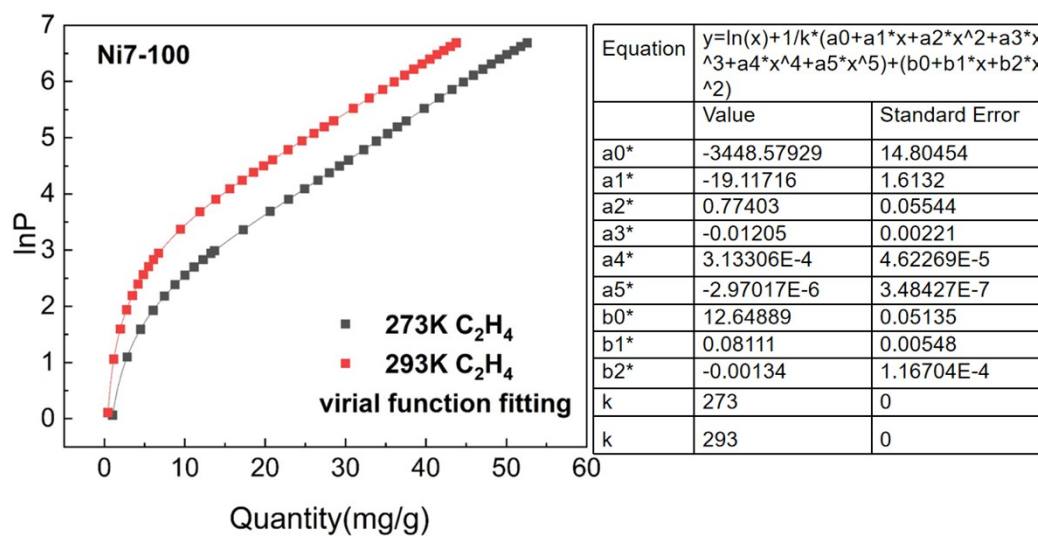| Equation | y=ln(x)+1/k*(a0+a1*x+a2*x^2+a3*x^3+a4*x^4+a5*x^5)+(b0+b1*x+b2*x^2) | |
|----------|--------|----------------|
|  | Value | Standard Error |
| a0* | -3448.57929 | 14.80454 |
| a1* | -19.11716 | 1.6132 |
| a2* | 0.77403 | 0.05544 |
| a3* | -0.01205 | 0.00221 |
| a4* | 3.13306E-4 | 4.62269E-5 |
| a5* | -2.97017E-6 | 3.48427E-7 |
| b0* | 12.64889 | 0.05135 |
| b1* | 0.08111 | 0.00548 |
| b2* | -0.00134 | 1.16704E-4 |
| k | 273 | 0 |
| k | 293 | 0 |

**Fig. S3** The $C_2H_4$ fit isotherms of Ni7-100 at 273 K and 293 K by virial equation.

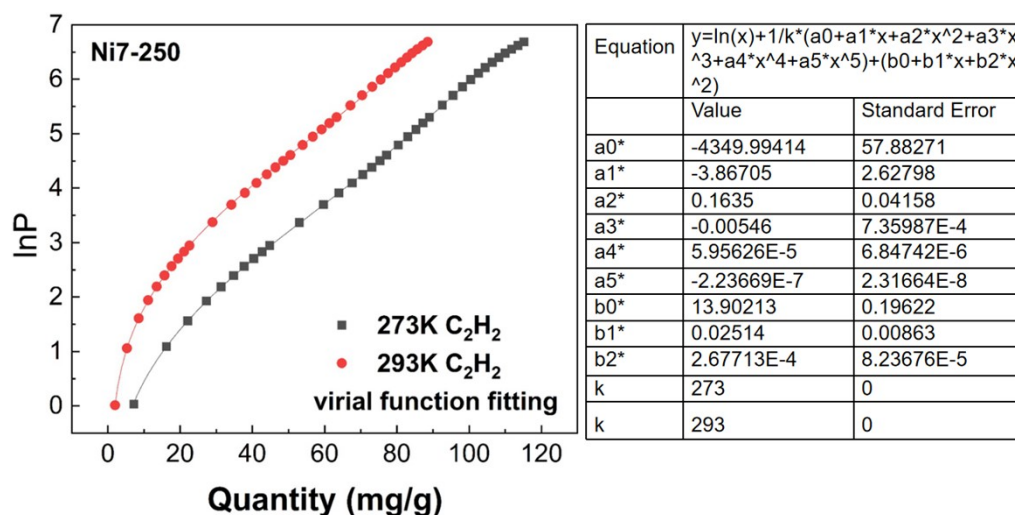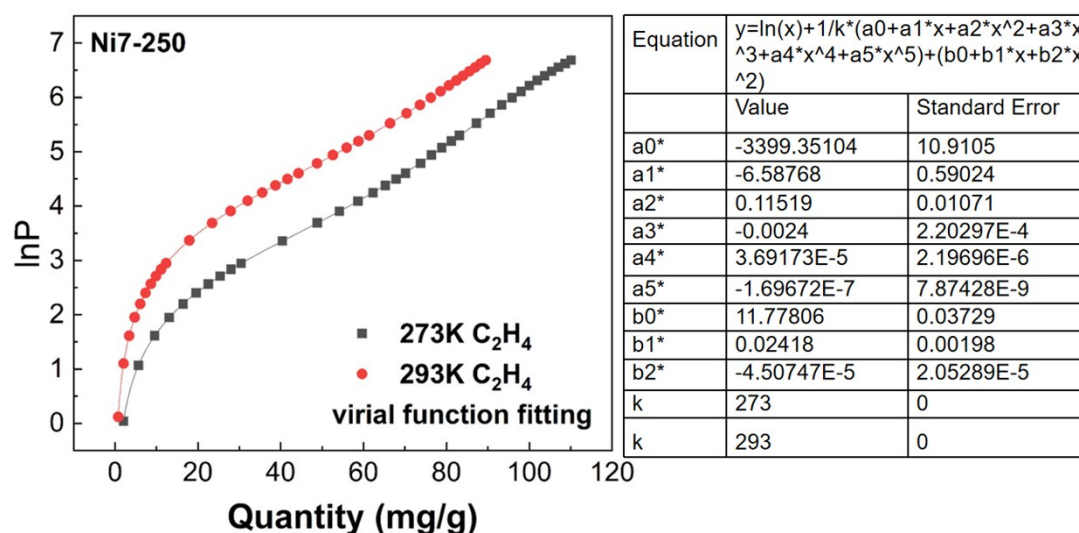**Fig. S4** The $C_2H_2$ fit isotherms of Ni7-250 at 273 K and 293 K by virial equation.
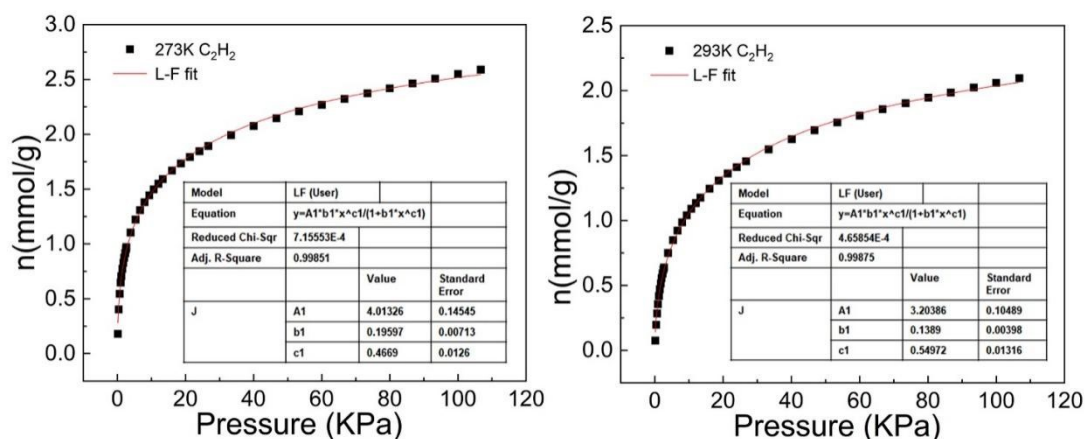
| Equation | $y=\ln(x)+1/k*(a0+a1*x+a2*x^2+a3*x^3+a4*x^4+a5*x^5)+(b0+b1*x+b2*x^2)$ | |
|---|---|---|
| | Value | Standard Error |
| a0* | -4349.99414 | 57.88271 |
| a1* | -3.86705 | 2.62798 |
| a2* | 0.1635 | 0.04158 |
| a3* | -0.00546 | 7.35987E-4 |
| a4* | 5.95626E-5 | 6.84742E-6 |
| a5* | -2.23669E-7 | 2.31664E-8 |
| b0* | 13.90213 | 0.19622 |
| b1* | 0.02514 | 0.00863 |
| b2* | 2.67713E-4 | 8.23676E-5 |
| k | 273 | 0 |
| k | 293 | 0 |



**Fig. S5** The $C_2H_4$ fit isotherms of Ni7-250 at 273 K and 293 K by virial equation.

| Equation | $y=\ln(x)+1/k*(a0+a1*x+a2*x^2+a3*x^3+a4*x^4+a5*x^5)+(b0+b1*x+b2*x^2)$ | |
|---|---|---|
| | Value | Standard Error |
| a0* | -3399.35104 | 10.9105 |
| a1* | -6.58768 | 0.59024 |
| a2* | 0.11519 | 0.01071 |
| a3* | -0.0024 | 2.20297E-4 |
| a4* | 3.69173E-5 | 2.19696E-6 |
| a5* | -1.69672E-7 | 7.87428E-9 |
| b0* | 11.77806 | 0.03729 |
| b1* | 0.02418 | 0.00198 |
| b2* | -4.50747E-5 | 2.05289E-5 |
| k | 273 | 0 |
| k | 293 | 0 |



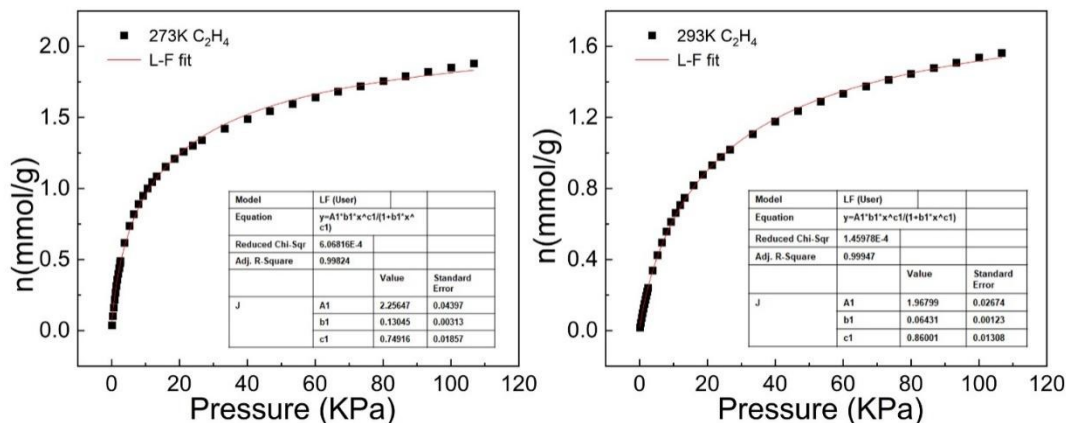**Fig. S6** The $C_2H_2$ fit isotherms of Ni7-100 at 273 K and 293 K by L-F model.

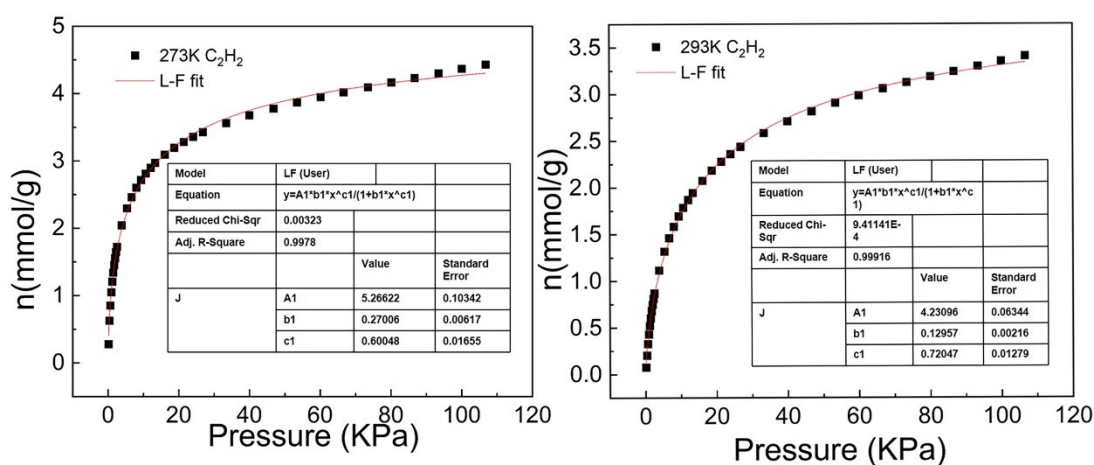**Fig. S7** The $C_2H_4$ fit isotherms of Ni7-100 at 273 K and 293 K by L-F model.



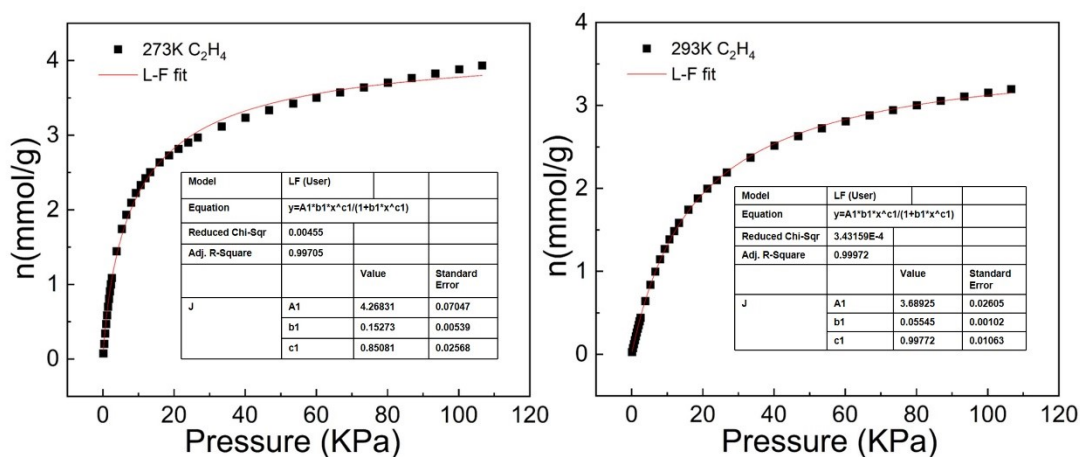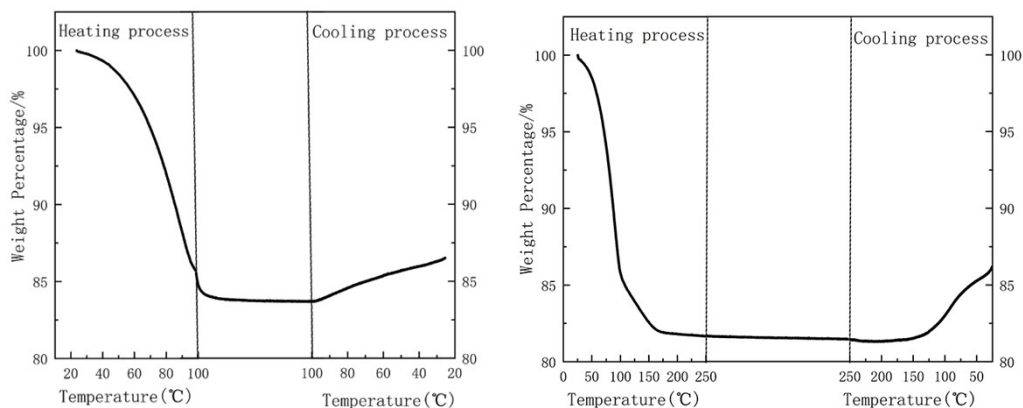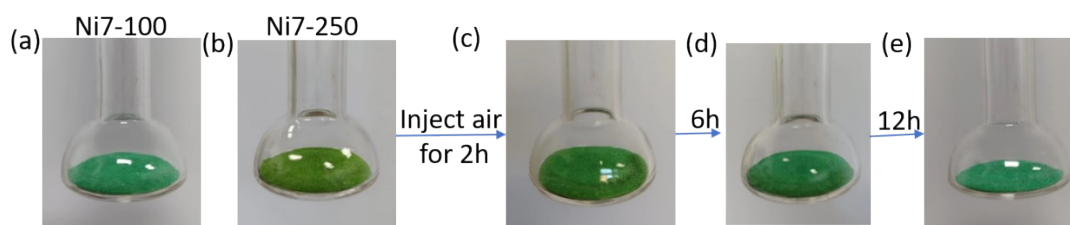**Fig. S8** The $C_2H_2$ fit isotherms of Ni7-250 at 273 K and 293 K by L-F model.



**Fig. S9** The $C_2H_4$ fit isotherms of Ni7-250 at 273 K and 293 K by L-F model.

**Fig. S10** The mass change chart for Ni7-MOF, under air protection, heated at a rate of 10K/min to 100°C (left) and 250°C (right), followed by a 6-hour isothermal hold before cooling down to room temperature.
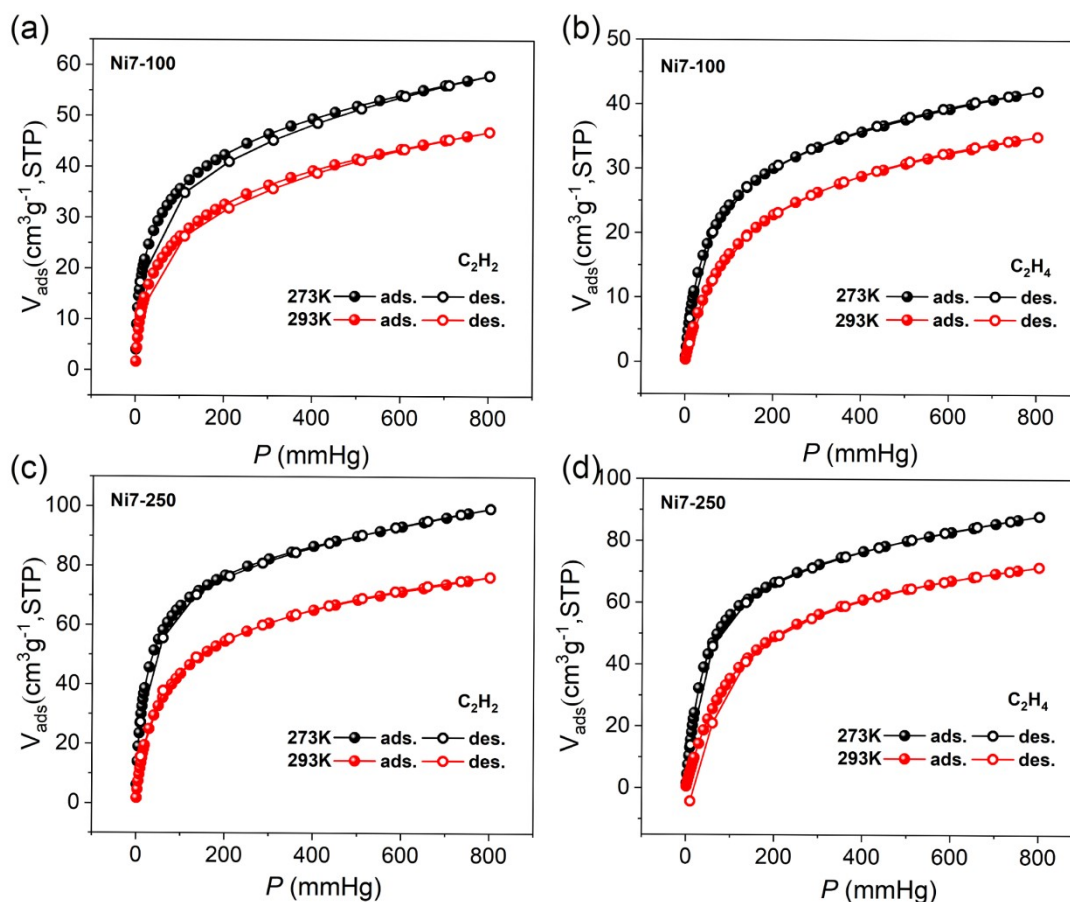


**Fig. S11** Crystallographic images of Ni7-100 (a) and Ni7-250(b). (c) to (e) illustrate the color alteration progression of Ni7-250 upon exposure to air for varying lengths of time.
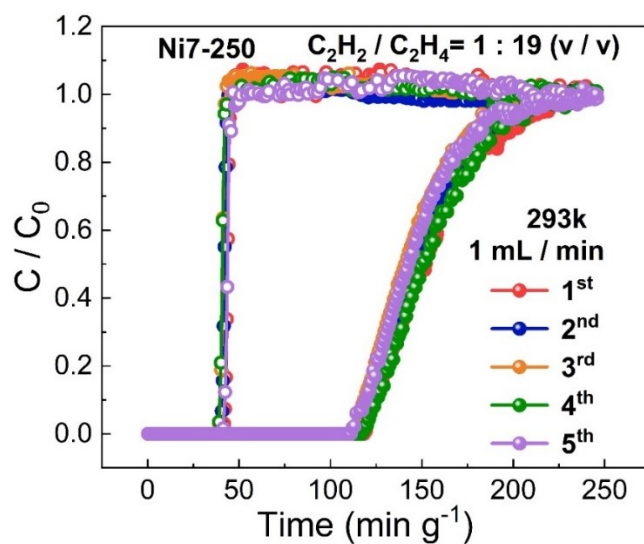


**Fig. S12** Breakthrough experiment cyclability for the $C_2H_2/C_2H_4$ (1/19, v/v) mixture with a gas flow rate of 1 mL min^{-1} at 293 K.

**Fig. S13** Single-component $C_2H_2$ and $C_2H_4$ adsorption and desorption curves of the two guest-free materials.

**Table S1** $C_2H_2$ adsorption capacity and $C_2H_2$ selectivity with other benchmark materials with similar BET surface areas.

| MOF | $S_{BET}$ (m² g⁻¹) | uptake(cm³ g⁻¹) | | $Q_{st}$(kJ mol⁻¹) | | selectivity for $C_2H_2/C_2H_4$ | Ref. |
|---|---|---|---|---|---|---|---|
| | | $C_2H_2$ | $C_2H_4$ | $C_2H_2$ | $C_2H_4$ | | |
| Ni7-100 | 177.08 | 46.15 | 34.42 | 32.81 | 28.67 | 4.24 | This work |
| Ni7-250 | 502.48 | 75.06 | 70.62 | 36.16 | 28.26 | 1.87 | This work |
| BSF-1 | 535 | 52.6 | 36.6 | 31.0 | 26 | 2.3 | 1 |
| MUF-17 | 247 | 67.0[a] | 48.0[a] | 49.5 | 31.1 | 8.7 | 2 |
| BSF-3 | 458 | 80.42 | 53.09 | 42.7 | 28.1 | 8.0 | 3 |
| SNNU-333-Ni | 519 | 51.2 | 27.5 | 33.8 | 32.3 | 4.4 | 4 |
| NUM-11 | 374.2 | 50.5 | 35.8 | 18.2 | 18 | 1.6[b] | 5 |
| JCM-1 | 550 | 75 | 35 | 36.9 | 34.2 | 13.2 | 6 |
| NTU-73-CH₃ | 1077.6 | 98.02 | 77.81 | 37.06 | 29.90 | 3.23 | 7 |
| NUM-15a | 721.65 | 78 | 55.14 | 37.4 | 33.2 | 2.4[b] | 8 |

| | | | | | | | |
|---|---|---|---|---|---|---|---|
| Zn-atz-oba | 710.7 | 62.048 | 45.47 | 27.5 | 27 | 1.43 | 9 |
| UPC-80 | 431 | 77.28 | 50.44 | 20.84 | 17.64 | 4.78 | 10 |
| UPC-22 | 486.3 | 37.4 | 24.2 | 21.1 | 15.9 | 2.6[b] | 11 |
| UiO-67-$(NH_2)_2$ | 2815 | 132.2 | 96.77 | 27.4 | 24.5 | 2.1 | 12 |
| NUM-9a | 330 | 52.1 | 49.9 | 35.8 | 32.3 | 1.5[c] | 13 |
| Cu(OH)INA | 206 | 48.3 | 31.8 | 36.1 | 29.6 | 41[b] | 14 |
| FJUT-1 | 1240 | 133.2 | 106.5 | 43.75 | 31.01 | 4.07[b] | 15 |
| SIFSIX-2-Cu-i | 503 | 90 | 49.1 | 41.9 | - | 44.5[b] | 16 |
| SIFSIX-3-Zn | 250 | 81.5 | 50.2 | 31.0 | - | 8.8[b] | 16 |
| SIFSIX-1-Cu | 1178 | 190.4 | 92.1 | 37.0 | - | 10.6[b] | 17 |
| ZU-901 | 135 | 40.32 | 14.8 | 45 | - | 83[d] | 18 |

a:Gas uptake at 293K   b:$C_2H_2$/$C_2H_4$=1/99   c: Gas uptake at 313K d: Gas uptake at 298 K, 0.01bar.

Reference:

(1) Y. Zhang, L. Yang, L. Wang, S. Duttwyler, H. Xing, A Microporous Metal-Organic Framework Supramolecularly Assembled from a Cu[II] Dodecaborate Cluster Complex for Selective Gas Separation, *Angew. Chem. Int. Ed.*, **2019,** *58,* 8145-8150.

(2) O. T. Qazvini, R. Babarao, S. G. Telfer, Multipurpose Metal-Organic Framework for the Adsorption of Acetylene: Ethylene Purification and Carbon Dioxide Removal, *Chem. Mater.,* **2019,** *31*, 4919-4926.

(3) Y. B. Zhang, J. B. Hu, R. Krishna, L. Y. Wang, L. F. Yang, X. L. Cui, S. Duttwyler and H. B. Xing, Rational Design of Microporous MOFs with Anionic Boron Cluster Functionality and Cooperative Dihydrogen Binding Sites for Highly Selective Capture of Acetylene, *Angew. Chem. Int. Ed.,* **2020**, 59, 17664 – 17669

(4) J. Zhang, Y. Y. Xue, P. Zhang, H. P. Li, Y. Wang, J. Xu, S. N. Li, and Q. G. Zhai, Honeycomb-Like Pillar-Layered Metal−Organic Frameworks with Dual Porosity for Efficient $C_2H_2$/$CO_2$ and $C_2H_2$/$C_2H_4$ Separations, *Cryst. Growth Des.*, **2022**, 22, 469−477

(5) S. Q. Yang, L. Zhou, Y. He, R. Krishna, Q. Zhang, Y. F. An, B. Xing, Y. H. Zhang, and T. L. Hu, Two-Dimensional Metal−Organic Framework with Ultrahigh Water Stability for Separation of Acetylene from Carbon Dioxide and Ethylene, *ACS Appl. Mater. Interfaces,* **2022**, *14,* 33429-33437.

(6) J. Lee, C. Y. Chuah, J. Kim, Y. Kim, N. Ko, Y. Seo, K. Kim, T. H. Bae, and E. Lee, Separation of Acetylene from Carbon Dioxide and Ethylene by a Water-Stable Microporous Metal–Organic

Framework with Aligned Imidazolium Groups inside the Channels, *Angew. Chem. Int. Ed.*, **2018**, 57, 7869 –7873

(7) Y. Li, Y. X. Wu, J. X. Zhao, J. G. Duan and W. Q. Jin, Systemic regulation of binding sites in porous coordination polymers for ethylene purification from ternary C2 hydrocarbons, *Chem. Sci.,* **2024**, 15, 9318–9324

(8) Q. Zhang, L. Zhou, P. Liu, L. Li, S. Q. Yang, Z. F. Li, T. Liang, Integrating tri-mural nanotraps into a microporous metal-organic framework for $C_2H_2/CO_2$ and $C_2H_2/C_2H_4$ separation, *Separation and Purification Technology*, **2022**, 296, 121404-121411.

(9) J. W. Cao, S. Mukherjee, T. Pham, Y. Wang, T. Wang, T. Zhang, X. Jiang, H.-J. Tang, K. A. Forrest, B. Space, M. J. Zaworotko, and K. J. Chen, One-step ethylene production from a fourcomponent gas mixture by a single physisorbent, *Nat. Commun.*, **2021**, 12, 6507

(10) C. H. Jiang, C. L. Hao, X. K. Wang, H. Y. Liu, X. F. Wei, H. K. Xu, Z. F. Wang, Y. Ouyang, W. Y. Guo, F. N. Dai, D. F. Sun, Constructing $C_2H_2$ anchoring traps within MOF interpenetration nets as $C_2H_2/CO_2$ and $C_2H_2/C_2H_4$ bifunctional separator, *Chemical Engineering Journal*, **2023**, 453, 139713

(11) X. P. Liu, Y. Li, C. L. Hao, W. D. Fan, W. Liu, J. Q. Liu, and Y. J. Wang, Optimizing the pore space of a robust nickel-organic framework for efficient $C_2H_2/C_2H_4$ separation, *Inorg. Chem. Front.,* **2023,** *10,* 824-831.

(12) X. W. Gu, J. X. Wang, E. Wu, H. Wu, W. Zhou, G. Qian, B. Chen, B. Li, Immobilization of Lewis Basic Sites into a Stable Ethane-Selective MOF Enabling One-Step Separation of Ethylene from a Ternary Mixture, *J. Am. Chem. Soc.,* **2022,** *144,* 2614-2623.

(13) S. Q. Yang, F. Z. Sun, P. Liu, L. Li, R. Krishna, Y. H. Zhang, Q. Li, L. Zhou, T. L. Hu, Efficient Purification of Ethylene from C2 Hydrocarbons with an $C_2H_6/C_2H_2$-Selective Metal-Organic Framework, *ACS Appl. Mater. Interfaces,* **2021,** *13,* 962-969.

(14) X. Zhang, Q. C. Chen, X. F. Bai, Y. L. Zhao, J. R. Li, Achieving Record $C_2H_2$ Packing Density for Highly Efficient $C_2H_2/C_2H_4$ Separation with a Metal-Organic Framework Prepared by a Scalable Synthesis in Water, *Angew. Chem. Int. Ed.,* **2024**, e202411744

(15) L. Zhang, T. T. Xiao, X. Y. Zeng, J. J. You, Z. Y. He, C. X. Chen, Q. T. Wang, A. Nafady, A. M. Al-Enizi, and S. Q. Ma, Isoreticular Contraction of Cage-like Metal–Organic Frameworks with Optimized Pore Space for Enhanced $C_2H_2/CO_2$ and $C_2H_2/C_2H_4$ Separations, *J. Am. Chem. Soc.,*

**2024**, 146, 11, 7341–7351.

(16) X. L. Cui, K. J. Chen, H. B. Xing, Q. W. Yang, R. Krishna, Z. B. Bao, H. Wu, W. Zhou, X. L. Dong, Y. Han, B. Li, Q. L. Ren, M. J. Zaworotko, B. L. Chen, Pore chemistry and size control inhybrid porous materials for acetylenecapture from ethylene, *Science*, **2016**, 353, 141-144.

(17) S. D. Burd, S. Q. Ma, J. A. Perman, B. J. Sikora, R. Q. Snurr, P. K. Thallapally, J. Tian, L. Wojtas, and M. J. Zaworotko, Highly Selective Carbon Dioxide Uptake by [Cu(bpy-n)2(SiF6)] (bpy-1 = 4,4′-Bipyridine; bpy-2 = 1,2-Bis(4-pyridyl)ethene), *J. Am. Chem. Soc.,* **2012**, 134, 3663−3666

(18) Z. D. Guo, L. F. Yang, Y. J. Li, J. Y. Cui, X. F. Lu, L. Y. Chen, X. Suo, X. L. Cui, and H. B. Xing, Pore-Environment Engineering of Pillared Metal−Organic Frameworks for Boosting the Removal of Acetylene from Ethylene, *Ind. Eng. Chem. Res.,* **2024**, 63, 8751−8760